DOI: 10.13009/EUCASS2023-539
Aerospace Europe Conference 2023 – 10TH EUCASS – 9TH CEAS

Two-phase pumped cooling system for power electronics; analyses and experimental results

Henk Jan van Gerner[1†], Arne K. te Nijenhuis[2†], Changmin Cao[3], Ignacio Castro[4], Douglas A. Pedroso[5], Herol Dsouza[6],

† Corresponding authors
[1] NLR - Netherlands Aerospace Centre, Marknesse, The Netherlands, henk.jan.van.gerner@nlr.nl
[2] NLR - Netherlands Aerospace Centre, Marknesse, The Netherlands, arne.te.nijenhuis@nlr.nl
[3] Collins-ART, Cork, Ireland, changmin.cao@collins.com
[4] Collins-ART, Cork, Ireland, ignacio.castro@collins.com
[5] Collins-ART, Cork, Ireland, douglasaraujo.pedroso@collins.com
[6] Collins-ART, Cork, Ireland, herol.dsouza@collins.com

Abstract

With the introduction of hybrid-electric propulsion, the amount of electrical power in the next generation of aircraft dramatically increases compared to current architectures. In the EU-funded H2020 EASIER project, the usage of two-phase mechanically pumped loops (MPLs) for cooling of power electronics is analysed. Ammonia and R1233zd(E) appear as premier candidates for aircraft two-phase cooling systems. In this study, an additively manufactured AlSi10Mg coldplate is manufactured and tested, which serves as interface between a DC/DC converter with 4 kW heat dissipation and a cooling fluid. Successful experimental validation of this evaporator is achieved in NLR's two-phase test facility.

1. Introduction

Hybrid electric propulsion dramatically increases the electrical power in the aircraft. As a result, the heat dissipation from electrical components will be an order of magnitude higher than for conventional aircraft, even if high levels of efficiency are achieved. Electronics in traditional turbofan-powered aircraft are cooled by air cooling. This cooling air is supplied by the Air Cycle Machine (ACM) that is driven by bleed air from a compressor stage of the aircraft engine. Large diameter air ducts are used to transport the cooling air to the electronic components. However, in electric aircraft, air cooling of the power electronics is not possible because the increased amount of waste heat would result in excessively large air ducts. Also, bleed air to power the ACM is not available anymore. Instead, novel mechanically pumped fluid cooling systems have to be developed to cool the power electronics. Because fluid cooling is more efficient than air cooling, relatively warm ambient air can be used to cool the electronics, instead of cold air from the environmental control system (ECS). This reduces the energy consumption of the ECS. Also, large air ducts to the electronic boxes can be replaced with small diameter fluid tubing. This results in system mass and volume reduction.

1.1. What is a two-phase pumped cooling system?

A two-phase MPL is similar to a liquid MPL, except that in a two-phase MPL, the liquid partially evaporates while it absorbs heat. Figure 1 shows a schematic drawing of a two-phase MPL. A pump transports liquid to an evaporator. In the evaporator, the waste heat from the power electronics is absorbed and the liquid partially turns into vapour. The vapour/liquid mixture then flows to the condenser. In the condenser, the absorbed heat from the power electronics is transferred to the ambient air via a ram air heat exchanger, and the vapour is condensed to liquid. The pressure and temperature of a two-phase fluid are coupled. As a result, the temperature of the liquid/vapour mixture is the same in the entire system (assuming a negligible pressure drop), and independent of the heat input.

Two-phase MPLs have several advantages compared to a liquid (e.g. water-eglycol) MPL:

- The fluid temperature is independent of the heat load due to the isothermal evaporation process. This results in a uniform interface temperature of the power electronics.
- The required massflow is much smaller, typically in the order of 10 times. This results in a lower mass and lower electrical power for the pump.

DOI: 10.13009/EUCASS2023-539

- The two-phase flow heat transfer coefficient is much higher than the liquid flow heat transfer coefficient. This high heat transfer coefficient results in a smaller temperature difference between the fluid and the power electronics. As a result, a higher fluid temperature can be used, which results in a smaller air heat exchanger.
- The freezing point of fluids that are used for a two-phase cooling system is much lower than the freezing point of water-eglycol that is used for a liquid cooling system. As a result, there are no freezing issues with two-phase cooling systems.

A disadvantage compared to a liquid MPL is that the accumulator of a two-phase MPL has to be considerably larger. Also, leak tightness is more important, and the design is more complex.

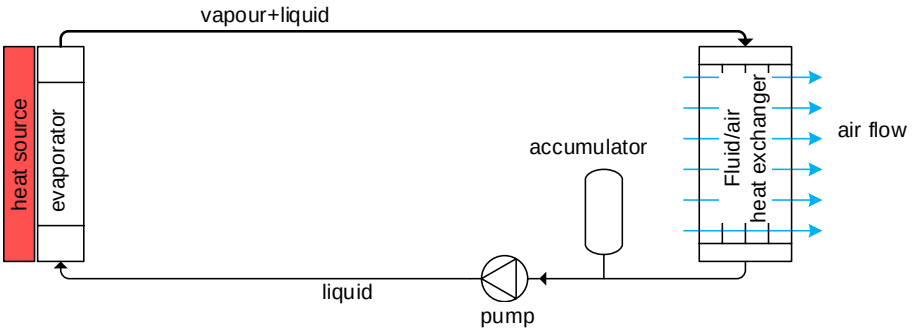

Figure 1: Schematic drawing of a two-phase MPL. The schematic of a liquid MPL is very similar, except that the fluid is in the liquid phase in the entire system.

1.2. Heat sources that are cooled with the pumped cooling system

In this paper, the focus is on cooling of the power electronics in an electric aircraft, since these have a high heat dissipation and heat flux, and are difficult to cool with other methods. The powertrain of the envisioned power train is comprised of an electric motor, AC power feeder, three-phase inverter based on an ANPC, and a DC/DC converter that connects to the battery. The boost converter and ANPC inverters are mounted on coldplates, as shown in Figure 2. The boost converter is comprised of four SiC power modules that generate a waste heat of 1015 W each. The heat flux of a single power module is 19.3 W/cm^2 (see Figure 3), resulting in a total heat dissipation for the boost converter of 4060 W. Each ANPC inverter has three SiC power modules. A typical heat amount of waste heat for the converters is 180 W for one power module and 210 W for the other two power modules on the ANPC, which amounts to a total of 600 W for a single ANPC inverter. Figure 3 shows a drawing of a single power module used in a boost converter and ANPC inverter.

The coldplate interface temperature has to be below 85°C in order to prevent overheating of the power electronics. The total amount of waste heat for the power electronics for one motor is 5860 W. The cooling system for the power electronics with a total amount of waste heat of 5860 W will be analysed in this project.

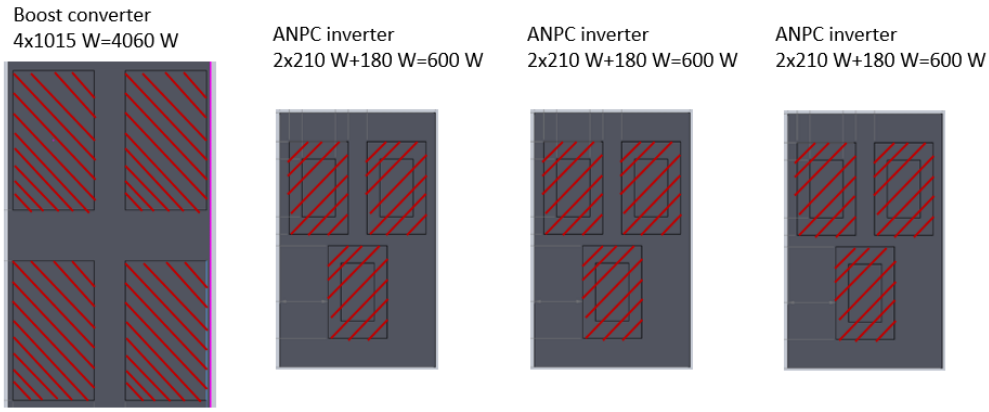

Figure 2: Schematic drawing of the four coldplates for the power electronics module for a single motor. The total amount of waste heat for the power electronics is 4060 W + 3 x 600 W = 5860 W.

DOI: 10.13009/EUCASS2023-539

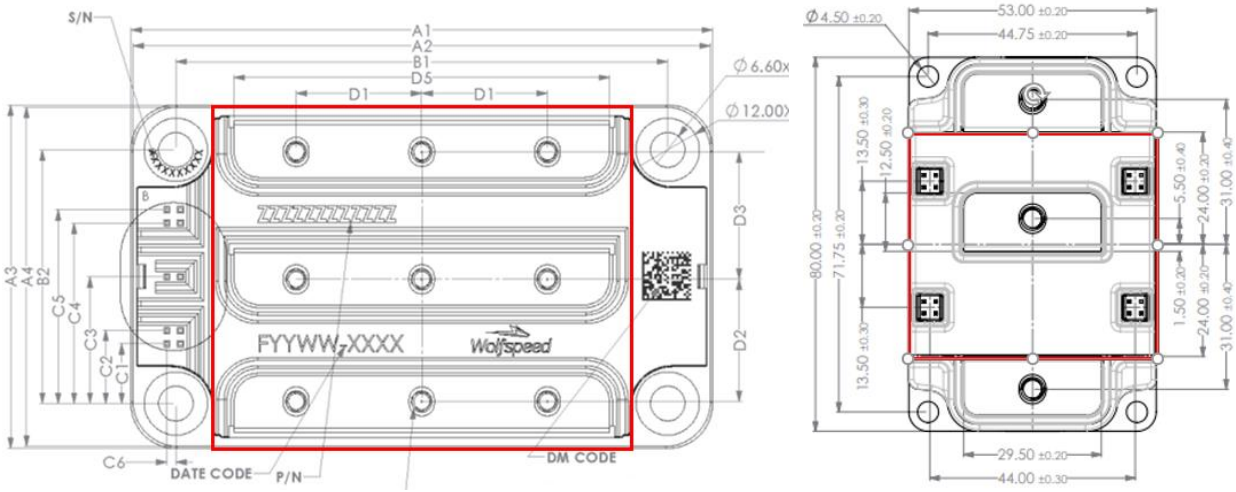

Figure 3: Drawing of a power module for a boost converter (left) and for an ANPC inverter (right). The waste heat is primarily generated within the rectangle indicate with the red line, which has an area of 8.1 cm x 6.5 cm = 52.65 cm^2 for the boost converter (resulting in a heat flux of 19.3 W/cm^2) and 4.8 cm x 5.3 cm = 25.44 cm^2 for the ANPC inverter (resulting in a heat flux of 8.3 W/cm^2).

1.3. Heat sink for the pumped cooling system

The waste heat generated by the power electronics has to be transported to a heat sink. In electric aircraft, the heat sink is the ambient air outside the aircraft. This air can have a temperature between -55°C and +50°C, for a CS-23B type aircraft. This air is routed through a ram air heat exchanger. When the aircraft is stationary, a fan is typically used to force air through the heat exchanger.

2. Two-phase fluid preselection

The selection of a suitable fluid is one of the first and most important steps for the design of a thermal control system. The number of fluids to choose from is very large. For example, the NIST Reference Fluid Thermodynamic and Transport Properties Database REFPROP [1] contains around 149 different fluids. Since the fluid properties vary with temperature, a fluid that show good performance at a certain temperature may not be suitable at another temperature. This is especially relevant for aerospace systems, since the operating fluid temperature for these systems (60°C to 100°C) is very different from the temperature range in typical terrestrial applications (e.g. -30°C for refrigeration systems and 10°C for air conditioning systems). For this reason, suitable fluids are pre-selected based on the 'figure of merit' for fluids.

2.1. Figure of merit

For a two-phase thermal management system, it is important that the tubing has a small diameter. Not only is the routing of the tubing much simpler when the diameter is small, but the system volume also scales with the square of the diameter, and a higher system volume results in larger and heavier components. For this reason, it is important to minimize the diameter of the tubing. However, a small diameter of the tubing results in a large pressure drop. This pressure drop is not only disadvantageous for the pump power, but large pressure gradients in a two-phase cooling system also result in large temperature gradients, since the fluid pressure and temperature are coupled in a two-phase cooling system. For this reason, an important characteristic of the fluid for two-phase thermal control system is a small pressure drop for the required heat transport and geometry.
The pressure drop in the liquid tubes can be calculated by the Darcy-Weisbach equation [2]:

$$\Delta p_l = f_l \frac{L}{d} \frac{\rho_l v_l^2}{2} \text{ with } v_l = \frac{\dot{m}}{\rho_l \pi d^2 / 4} \text{ and } \dot{m} = \frac{P}{h_{lv}} \quad \textbf{(1)}$$

The flow in the tubes is turbulent, and the friction factor can be approximated with the Blasius correlation for turbulent flow in smooth-walled tubes:

DOI: 10.13009/EUCASS2023-539

$$f_l = \frac{0.3164}{\mathrm{Re}_l^{0.25}} \tag{2}$$

The same equations can be used for the vapour tubes, when the subscript *l* is replaced by *v*. In order to find a fluid with a small pressure drop, Eq. (1) and Eq. (2) are rearranged to (assuming that half of the fluid is liquid and half is vapour):

$$\Delta p \propto \overbrace{\left(\frac{\mu_l^{1/4}}{\rho_l h_{lv}{}^{7/4}} + \frac{\mu_v^{1/4}}{\rho_v h_{lv}{}^{7/4}} \right)}^{\text{fluid-dependent}} \overbrace{\frac{L}{d^{19/4}}}^{\text{geometry-dependent}} \overbrace{P^{7/4}}^{\text{Heat input}} \tag{3}$$

The equation for the pressure gradient in the system is rearranged in a fluid-dependent part, a geometry-dependent part (i.e. the length and diameter of a tube) and the heat input. The inverse of the fluid-dependent part in the equation above can be used to find a fluid that results in a small pressure gradient, named the Figure of Merit for low pressure drop:

$$M_{\text{low }\Delta p} = \frac{1}{(\mu_l^{1/4} / (\rho_l h_{lv}{}^{7/4}) + \mu_v^{1/4} / (\rho_v h_{lv}{}^{7/4}))} \quad \textit{Figure of Merit based on low pressure gradient} \tag{4}$$

2.2. NFPA fluid safety rating system

In the Fluid Selection Tool, the safety of a fluid is rated with the NFPA 704 standard [3]. This NFPA rating is divided in four categories which are color-coded with red indicating flammability, blue indicating level of health hazard, yellow for chemical instability, and white containing codes for special hazards. Each category of health, flammability and instability is rated on a scale from 0 (minimal hazard) to 4 (severe hazard). As an example, Figure 4 shows the NFPA 'safety diamond' for ammonia. In this stage of the project, it is not entirely clear what the maximum alowed safety rating is. However, there is a strong preference for a non-flammable (i.e. a NFPA rating for flammability of 1 or lower) and non-toxic (i.e. a NFPA rating for heatlth of 2 or lower) fluid. Unfortunately, flammable and/or toxic fluids generally have a better thermal performance than safer alternatives.

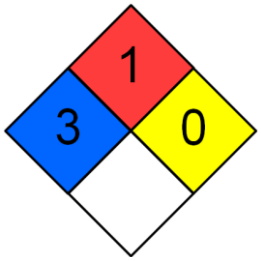

Figure 4: NFPA diamond for ammonia.

2.3. Fluid figure of merit for different NFPA ratings

Figure 5 shows the Figure of Merit *M* for all fluids in the REFPROP fluids database with a NFPA rating of 3 or lower, excluding the fluids that are banned according to the Montreal protocol. Also, all fluids with a freezing temperature above -55°C are excluded. On the horizontal axis, the saturation temperature of the fluid is shown. The fluid saturation temperature of the EASIER application is around 75°C. This temperature is indicated with the dashed grey vertical line. The Figure of Merit for ammonia is much higher than for any other fluid (e.g. an order of magnitude larger than for R134a). This means that the tubing diameter for a system with ammonia can be much smaller than for other fluids. Fluids with a NFPA rating of 4 (e.g. propyne, R40 or DME) are not shown in the figure, but all these fluids also have a much lower Figure of Merit than ammonia. Ammonia is commonly used in (industrial) cooling applications, but because of its toxicity (NFPA=3 for health), it is more difficult to use than other fluids. There are many fluids with a more favourable NFPA rating, i.e. a NFPA rating of 2 or lower, but these have a much lower Figure of Merit than ammonia. The Figure of Merit for fluids with a NFPA rating of 2 or lower are shown in Figure 6.

Table 1 shows the fluid properties for ammonia (which has a NFPA rating of 3), and the fluids with the highest Figure of Merit in NFPA category 2 or lower. Besides fluid properties, this table also shows some system characteristics that are calculated by the Fluid Selection Tool, namely the required volume flow, massflow and the required tube diameter. From the Figures of Merit, it can be seen that ammonia has about 16 times higher Figure of Merit than e.g. R245fa. This means that a system with ammonia would have a 16 times lower pressure drop than the same system that is filled with R245fa. Normally, a system with ammonia will have a smaller diameter tubing. The typical tubing diameter for a two-phase transport tube is calculated by the Fluid Selection Tool in order to get a rough indication of the tubing diameter. As can be seen from the table, the tube inner diameter with ammonia has to be 7.5 mm, while with R245fa

DOI: 10.13009/EUCASS2023-539

it has to be 13.9 mm in order to obtain a similar pressure drop in a system. The fluids in this table are analysed in more detail with the System Analysis Tool. This is described in the next section.

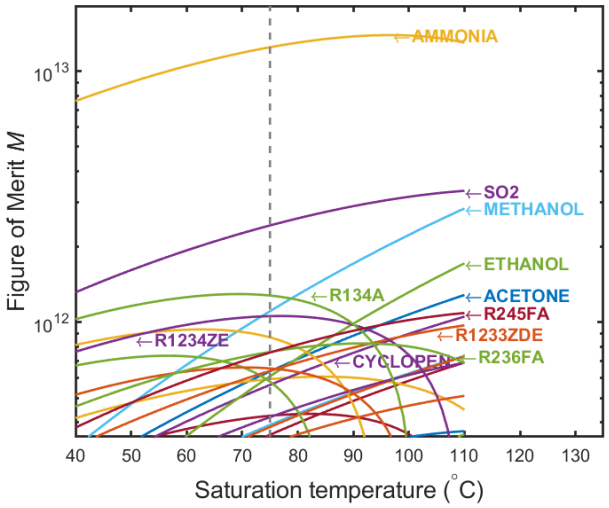

Figure 5: Figure of Merit for all fluids in the REFPROP database with a NFPA rating of 3 or lower.

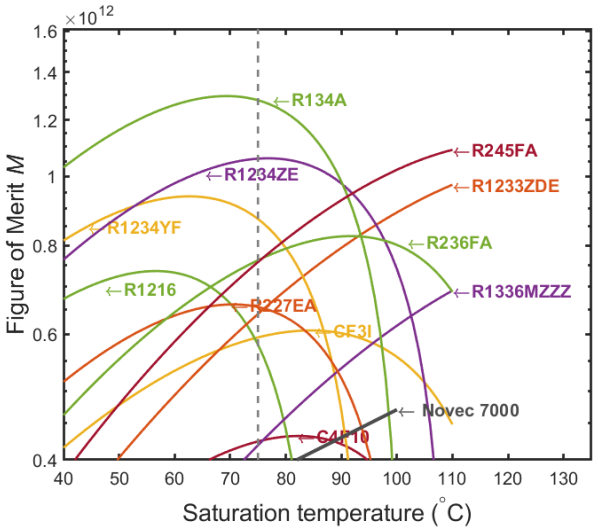

Figure 6: Figure of Merit for all fluids in the REFPROP database with a NFPA rating of 2 or lower.

Table 1: Relevant characteristics at 75°C for fluids with the highest Figure of Merit. The first NFPA number is for health, the second is for flammability. Blue entries mark fluid properties; red entries mark system characteristics.

	Ammonia	R134a	R1234ze	R245fa	R236fa	R1233zd(E)
NFPA [health, flammability]	3-1	1-0	2-1	2-1	1-0	2-0
Pressure at 75°C (barA)	37.1	23.6	18.0	6.9	11.0	5.8
Pressure at 20°C (barA)	8.6	5.7	4.3	1.2	2.3	1.1
Triple point (°C)	-78	-103	-104	-103	-93	-78
Heat of evaporation h_{lv} (kJ/kg)	909	116	118	158	111	161
Specific heat C_p (kJ/kgK)	5.6	1.9	1.7	1.5	1.4	1.3
Liquid density ρ_l (kg/m^3)	517	965	961	1188	1161	1130
$\partial T_{sat}/\partial p_{sat}$ (°C/bar)	1.2	1.9	2.5	5.5	3.8	6.8
Required massflow (g/s)	9.2	72.1	71.2	53.0	75.6	51.8
Required volume flow (lpm)	1.1	4.5	4.4	2.7	3.9	2.8
Typical inner diameter for two-phase tubing (mm)	7.5	12.3	12.9	13.9	13.9	14.4

3. Two-phase cooling system analysis

To make a trade-off between the pre-selected working fluids, a detailed steady-state simulation has been made with the NLR's in-house cooling system analysis tool.[4] [5]. This tool numerically solves (in MATLAB) the steady-state mass and enthalpy equations for a two-phase flow. The frictional pressure drop in the system is calculated with the Darcy–Weisbach equation in which the friction factor for turbulent flow is calculated with the Colebrook equation [2] and the friction factor for laminar flow is calculated by Re/64 [2]. For two-phase flow, the pressure drop is calculated with the Friedel correlation [6]. The flow's heat transfer coefficient is calculated with the Gnielinski correlation [2] for turbulent liquid flow, with the Kandlikar correlation for evaporating flow [7], and with the Shah correlation for condensing flow [8]. A detailed description of the Cooling System Analysis Tool is provided in reference [4] and [5]. All fluids in Table 1 have been analysed with the simulation tool. The results for ammonia and R1233zd(E) are described in more detail in the next sections. The results for the other fluids are only included in the summary table. From these calculations, the volume and mass of the system components can be estimated.

3.1. Results for ammonia

Figure 7 shows the calculated temperatures in the system, together with calculated system parameters. The input parameters for the model are indicated with red text, while the output is in black text. On the left side of the figure, the evaporators are located, while the condenser is on the right side of the figure. The horizonal arrows that cross the condenser indicate the ram air flow that cools the condenser. The arrows are coloured according to the air temperature.

DOI: 10.13009/EUCASS2023-539

The typical tubing inner diameter from table 1is used for the two-phase tubing, while the diameter of the liquid tubing is 2/3 times this value. The tubing length between the evaporator and the condenser is 8 m while the tubing length from the condenser to the pump and from the pump to the evaporator is 5 m. Figure 8 shows the calculated vapour mass fraction in the system, while Figure 9 shows the calculated pressure. From the calculated pressure plot, a pressure drop at the inlet of each evaporator branch can be observed. This pressure drop is caused by flow restrictions that are located at the inlet of each evaporator branch. These flow restrictions are used to correctly distribute the flow over the parallel branches.

The ram air heat exchanger is a cross-flow heat exchanger. The air enters the condenser with a temperature of 50°C. When the air flows through the condenser, it absorbs the heat from the fluid and the air warms to a temperature of 58°C at the air outlet near the condenser fluid inlet. The liquid leaves the condenser at a temperature very close to the inlet air temperature. Figure 10 shows the temperatures along the condenser. The ammonia enters the condenser as a vapour/liquid mixture with a temperature of 75°C. The fluid remains 75°C as it flows through the condenser, until all the vapour is condensed into liquid (approximately halfway in the condenser), after which the liquid temperature quickly drops. The heat transfer coefficient between the fluid and condenser wall is very high, which results in a very small temperature difference between ammonia and condenser. The temperature difference between the condenser wall and air is much larger, which means that the air heat exchange is the largest thermal resistance in the thermal path from fluid to air. The air heat exchanger in this simulation is over-dimensioned and could be made smaller.

The liquid enters the evaporator with a temperature of 51°C. In the evaporator, the temperature liquid quickly rises to the saturation temperature of 75°C, after which it starts to evaporate and remains constant in temperature while it absorbs the dissipated heat from the power electronics.

The volume of the accumulator is 1.5 times the volume of the system between the evaporator inlet and the condenser outlet (i.e. the part of the system where vapour can occur) plus the volume of the liquid needed for expansion due to temperature variations. The mass of the accumulator vessel is calculated assuming a maximum saturation temperature of 110°C in the accumulator. The mass calculation is based on the pressure strength of the vessel. Details on the mass calculation of the accumulator and other components can be found in section 3.3. The required pump power (W_{pump}) is calculated by assuming a pump efficiency of 50%. For ammonia, the calculated pump power is only 2 W.

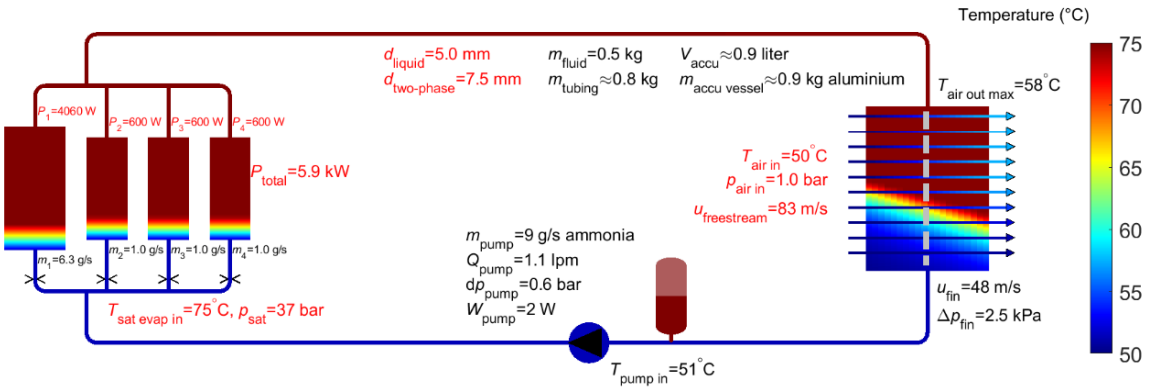

Figure 7: Calculated temperatures with ammonia. The temperature along the dashed grey line in the condenser is plotted in Figure 10.

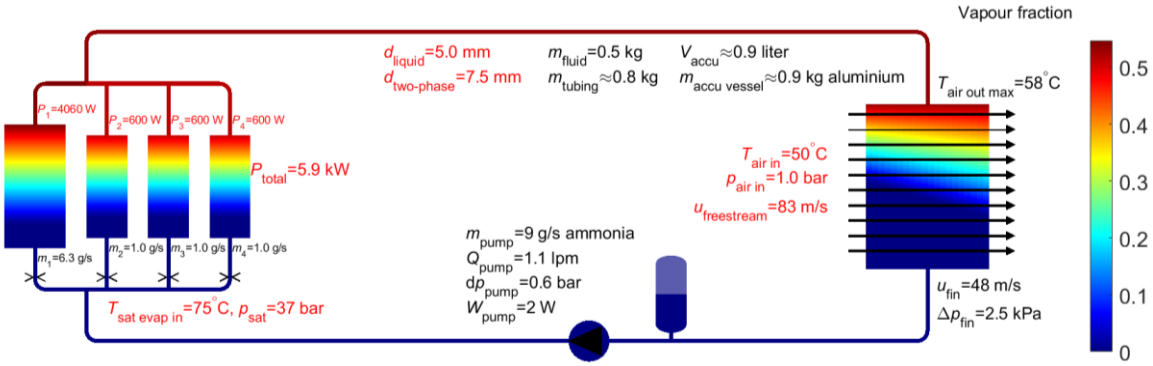

Figure 8: Calculated vapour mass fraction with ammonia.

DOI: 10.13009/EUCASS2023-539

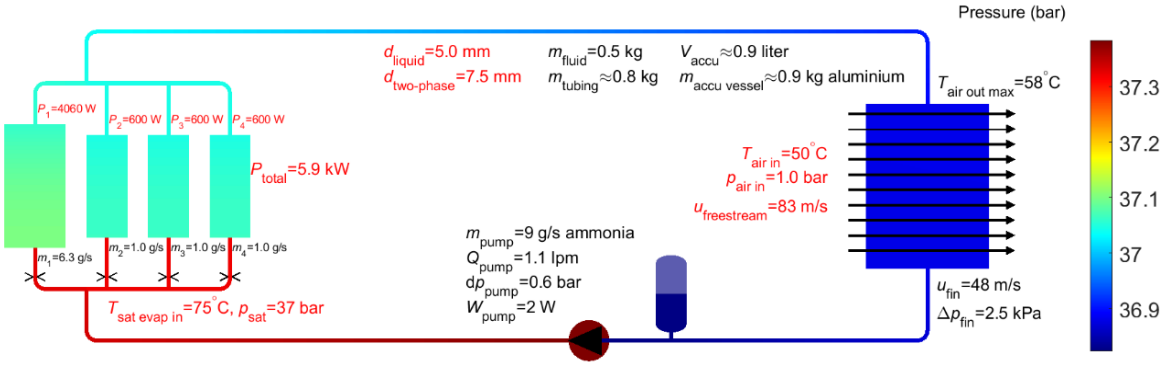

Figure 9: Calculated pressure with ammonia.

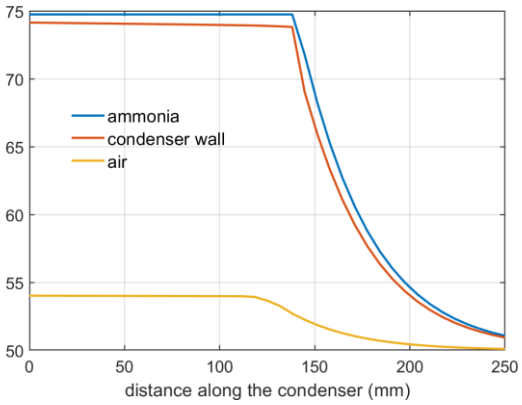

Figure 10: Calculated temperatures along the condenser, as indicated by the grey dashed line in Figure 7.

3.2. Results for R1233zd(E)

In this section, the results for R1233zd(E) are presented. The input and geometry files are exactly the same as for the simulation for ammonia (see Figure 7), except that the diameter for the tubing is changed from 7.5 mm into 14.4 (see table 1). The larger tubing diameter and higher liquid density for R1233zd(E) results in a 7 times higher fluid mass than for ammonia. The accumulator volume is approximately 2.6 litres, compared to the 0.9 litres needed for ammonia. The calculated mass of the vessel however is smaller than for ammonia, because of the lower saturation pressure of R1233zd(E). The required volume flow of 2.8 l/min for R1233zd(E) is 2.5 times larger than for ammonia. The pressure difference over the pump is similar, because the diameter of the tubing is chosen such that the pressure difference is similar. The heat transfer is less efficient for R1233zd(E) than for ammonia, which results in a higher liquid temperature at the condenser outlet. This means that the air heat exchanger for a system with ammonia can be smaller than the air heat exchanger for a system with R1233zd(E). The simulation results for R1233zd(E) and the other fluids are summarized in table 2 in section 3.6.

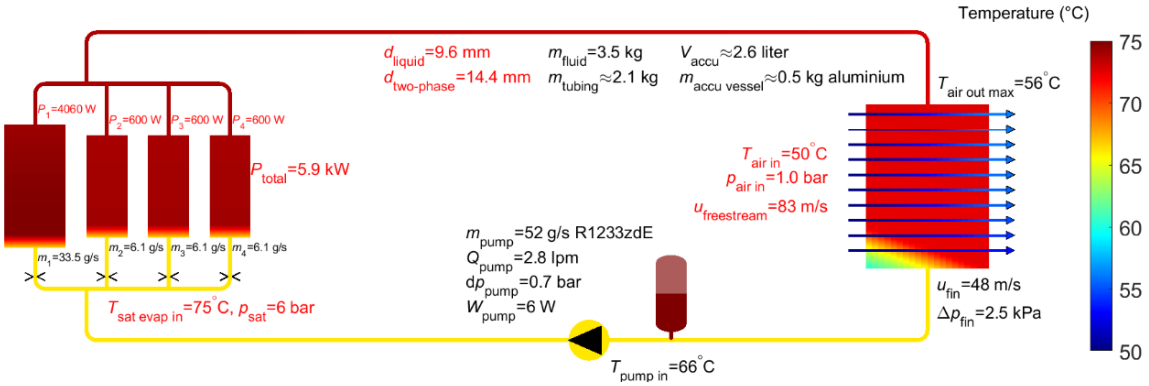

Figure 11: Calculated temperatures with R1233zd(E).

DOI: 10.13009/EUCASS2023-539

3.3. Mass estimation

In this section, the method for calculating the mass of several components is explained. The mass summary for different fluids is included in table in section 3.6.

Accumulator vessel
Figure 12 shows a schematic drawing of an accumulator vessel. It consists of a cylinder with two caps. In the simulations, it is assumed that the ratio between H_{cylinder} and D_{cylinder} is 1.5. The minimum volume of an accumulator is equal to the volume of the system between the evaporator inlet and the condenser outlet (i.e. the part of the system where vapour can occur) plus the volume of the liquid needed for expansion due to temperature variations. The actual volume of the accumulator has to be somewhat larger. In the analyses, it is assumed that that the accumulator volume is 1.5 times the minimum required volume. The volume of the accumulator consists of the volume of the cylinder, $V_{\text{cylinder}} = \frac{1}{4}\pi D_{\text{cylinder}}^2 H_{\text{cylinder}}$ and the volume of the spherical caps, $V_{\text{caps}} = \frac{1}{6}\pi D_{\text{cylinder}}^3$. From these equations, the required diameter and height of the accumulator are calculated. The wall thickness of the cylinder and caps of the vessel are then calculated with the pressure vessel equations:

$$t_{\text{wall, cylinder}} = \frac{p_{\text{proof/burst}}\, D_{\text{cylinder}}}{2\,\sigma_{\text{yield/ultimate}}}\, S_{\text{margin}}\ ,\ t_{\text{wall, caps}} = \frac{p_{\text{proof/burst}}\, D_{\text{cylinder}}}{4\,\sigma_{\text{yield/ultimate}}}\, S_{\text{margin}} \quad \textbf{(5)}$$

in which $p_{\text{proof/burst}}$ is the proof or burst pressure for the vessel. For the wall thickness calculation for the proof pressure, the yield strength σ_{yield} of the vessel wall is used, while for the wall thickness calculation for the burst pressure, the ultimate strength σ_{ultimate} is used. The factor S_{margin} is an additional safety margin. In the analysis, this margin is 1.2.

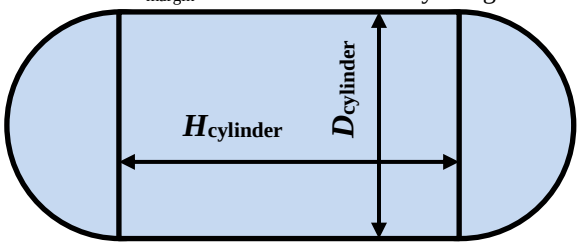

Figure 12: Schematic drawing of an accumulator vessel.

Tubing
The mass of the tubes is calculated with:

$$m_{\text{tube}} = L_{\text{tube}}\, \pi d_{\text{tube}}\, t_{\text{wall tube}}\, \rho \quad \textbf{(6)}$$

in which L_{tube} is the length of the tube, d_{tube} is its diameter, t_{wall} is the wall thickness of the tube, and ρ is the density of the tube wall. It assumed that aluminium tubes are used, so the density is 2700 kg/m^3. The thickness of the tube wall increases with the diameter. The thickness of the wall is approximated with:

$$t_{\text{wall tube}} = \frac{d_{\text{tube}}}{20} + 0.5\ \text{mm} \quad \textbf{(7)}$$

Fluid
The total fluid mass in the system is equal to the total volume of the system multiplied by the liquid density of the fluid.

Other components
It is assumed that the evaporators, air heat exchanger, and pump have approximately the same mass for all fluids, so these are not included in the comparison. Also, the mass of the brackets, frame, and other components are not included, since such details are not yet known in this stage of development of two-phase cooling systems for aircraft.

3.4. Material compatibility

Ammonia has an excellent compatibility with stainless steel 316 and many aluminium alloys (e.g. 6061 and 6063) Ammonia has a very poor compatibility with copper, so e.g. stainless-steel plate heat exchangers that are copper-brazed

DOI: 10.13009/EUCASS2023-539

cannot be used. Ammonia is not compatible with several common seal materials (e.g. Viton), but sufficient compatible seal materials are available (e.g. EPDM). All other fluids in table 1 have an excellent compatibility with aluminium, stainless steel, copper and titanium. Also, the compatibility with most seal materials is good.

3.5. Future availability of fluids

R134a, R245fa and R236fa are hydrofluorocarbons (HFCs) that were developed to replace ChloroFluoroCarbons (CFCs) and HydroChloroFluoroCarbons (HCFCs) that damage the ozone layer. CFCs and HCFCs are banned according to the Montreal protocol. R134a, R245fa and R236fa do not damage the ozone layer and are (almost) non-flammable, but they do have a high global warming potential (more than 150 times greater than carbon dioxide). EU regulations (e.g. the MAC directive) prohibit the use of fluorinated gases with a global warming potential of more than 150 times greater than carbon dioxide in all new cars and vans produced from 2017. As a result, R134a is not used anymore in the air-conditioning of new cars but has been replaced with other refrigerants, e.g. R1234ze. In all other applications, the hydrofluorocarbon fluids are being phased-out when alternatives are available. For example, R1233zd(E) is intended as a replacement for R245fa, so it is to be expected that R245fa will also be phased-out. This could mean that availability of these fluids in the far future could be an issue.
R1234ze and R1233zd(E) are HydroFluoroOlefins (HFOs) that have been developed as replacement for the HFCs. These fluids have a low global warming potential. However, these fluids are relatively new, and it might be too early to tell whether these fluids represent the long-term solution or not. For example, the German Environment Agency calls for a ban of R1233zd, since it has an ozone depletion potential of 0.00034 [11]. Also, recently concerns have been raised about the environmental impact of PFAS (Per- and polyfluoroalkyl substances) which might impact availability of these engineered refrigerants [12]. Ammonia (also known as refrigerant R717) is used on a wide scale in industrial refrigeration, but also in many other applications. No issues with future availably of ammonia are foreseen.

3.6. Summary and fluid selection

Table 2 shows the summary of the analysis results. Ammonia has large advantages compared to other fluids: the required volume flow of ammonia, the system mass, and the system volume are at least 2.5 times lower than for the other pre-selected fluids. However, ammonia has the highest NFPA rating due to its toxicity and mild flammability. As a result, the certification of a cooling system with ammonia will take much longer than for a system with a lower-NFPA fluid. Therefore, in this study, it was decided to only assess ammonia by modelling, and that for two-phase coldplate testing another fluid with shorter-term certification opportunities was chosen. For the remaining fluids in Table 2 R134a, R245fa, and R236fa are being phased-out because of their high Global Warming Potential (see previous section) and are therefore not considered. R1234ze and R1233zd(E) remain as suitable fluids for a two-phase cooling system. An advantage of R1233zd(E) is that a smaller pump volume flow is required. Also, R1233zd(E) is non-flammable, whereas R1234ze is mildly flammable. For these reasons, R1233zd(E) was selected in the EASIER project.

Table 2: Summary table for the fluid selection for a 5860 W cooling system.

Fluid	NFPA	Triple point (°C)	Volume flow (lpm)	inner tube diameter (mm)	System mass (kg)	Accumulator volume (liter)	Pump power (W)	Long term availability	GWP
Ammonia	3-1	-78	1.1	7.5	2.2	0.9	2	Good	0
R134a	1-0	-103	4.5	12.3	5.3	2.1	12	Phased-out	1530
R1234ze	2-1	-104	4.4	12.9	5.5	2.2	11	Probably good	1.4
R245fa	2-1	-103	2.7	13.9	5.9	2.4	6	Phased-out	962
R236fa	1-0	-93	3.9	13.9	6.3	2.5	10	Phased-out	8690
R1233zd(E)	2-0	-78	2.8	14.4	6.1	2.6	6	Probably good	3.9

4. Test of evaporator plate

In this paper, the focus is on cooling of the power electronics in an electric aircraft, since these have a relatively large amount of heat dissipation with a high heat flux. Therefore, they are difficult to cool with other cooling methods. For each motor, the power electronics has one boost converter and three ANPC inverters. The boost converter is the most challenging to cool, and for this reason, it was decided to design, manufacture and test a coldplate for the boost converter. The boost converter is comprised of four power modules that generate a waste heat of 1015 W each, resulting in a total of 4060 W. See Figure 3 for a schematic drawing of a single power module for a boost converter. The heat load of a power module is emulated by resistive heating elements embedded in a copper heater block, as shown in

DOI: 10.13009/EUCASS2023-539

Figure 13. This heater block can generate 1060 W of heat. Four heater blocks are mounted on a single coldplate, as discussed in the next section. Dow Corning TC-5026 thermal paste is used between the coldplate and the heater blocks.

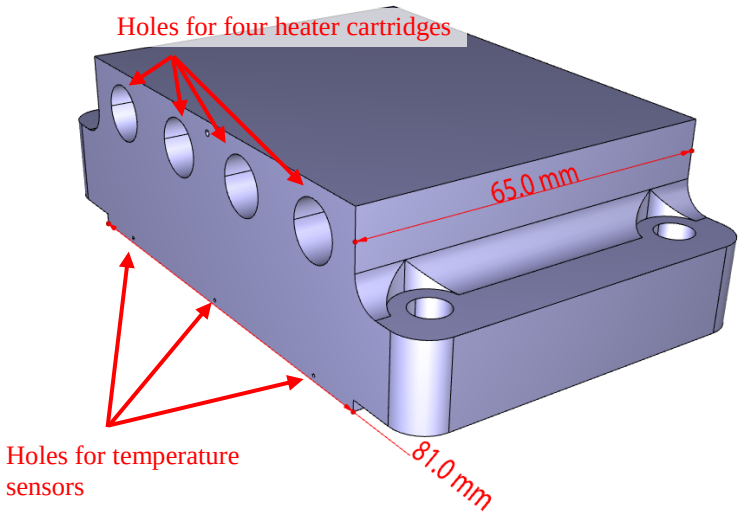

Figure 13: CAD drawing of a heater block that emulates the heat dissipation of a power module.

4.1. Evaporator design

Figure 14 shows a CAD drawing of the evaporator plate while Figure 15 and Figure 16 show CAD drawings of the plate with the heater blocks. The coldplate has 41 parallel channels with a diameter of 1.5 mm. Each heater block has 6 holes in which temperature sensors can be inserted, shown in Figure 13. These holes have a diameter of 0.6 mm and a depth of 10 mm, while the temperature sensors have a diameter of 0.5 mm. The evaporator plate is connected to the test setup with Stäubli SPH non-spill quick-connect fluid couplings. These couplings allow for an easy connect and disconnect of the coldplate. The couplings are closed when disconnected, so the fluid can remain in the system when the evaporator plate is disconnected. Figure 17 shows a photo of the evaporator plate with Stäubli couplings. The coldplate has been manufactured by metal additive manufacturing with AlSi10Mg and passed the proof pressure and helium leak-tightness tests.

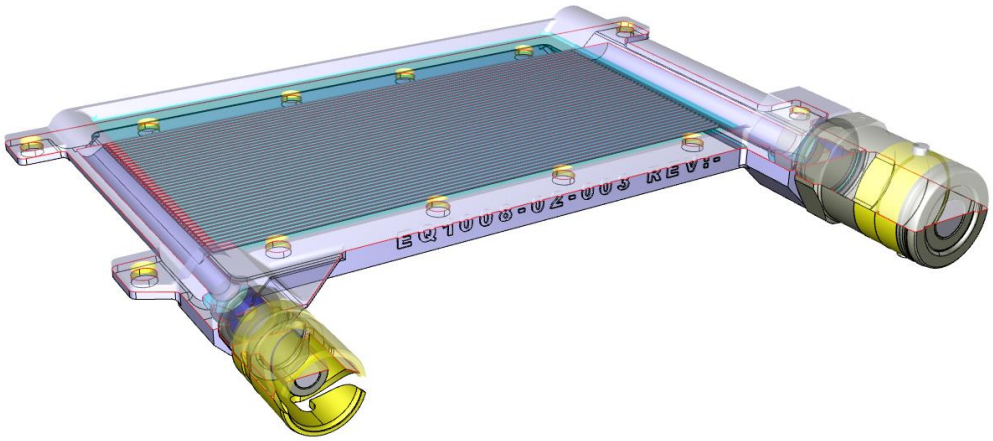

Figure 14: Cross section of the coldplate.

DOI: 10.13009/EUCASS2023-539

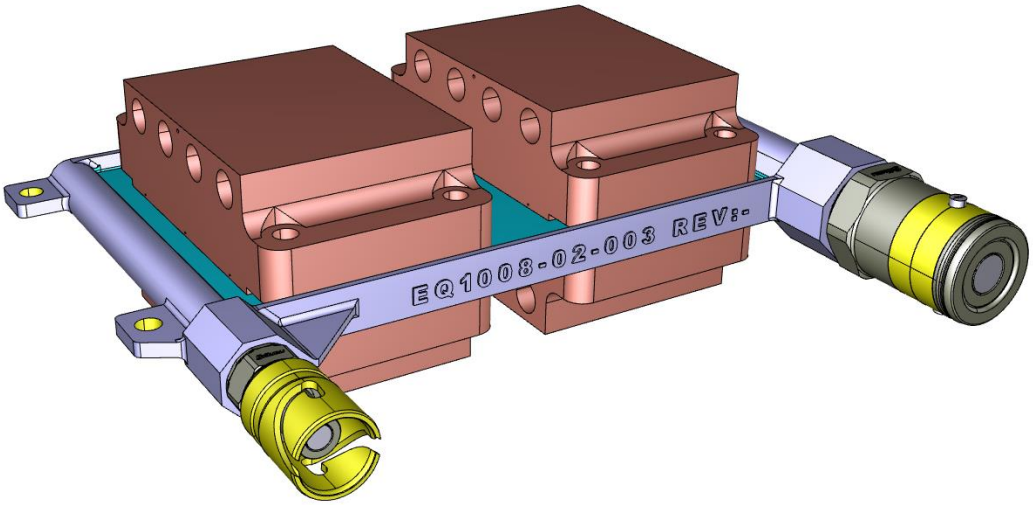

Figure 15: Coldplate with four heater blocks that emulate the heat dissipation of four power modules.

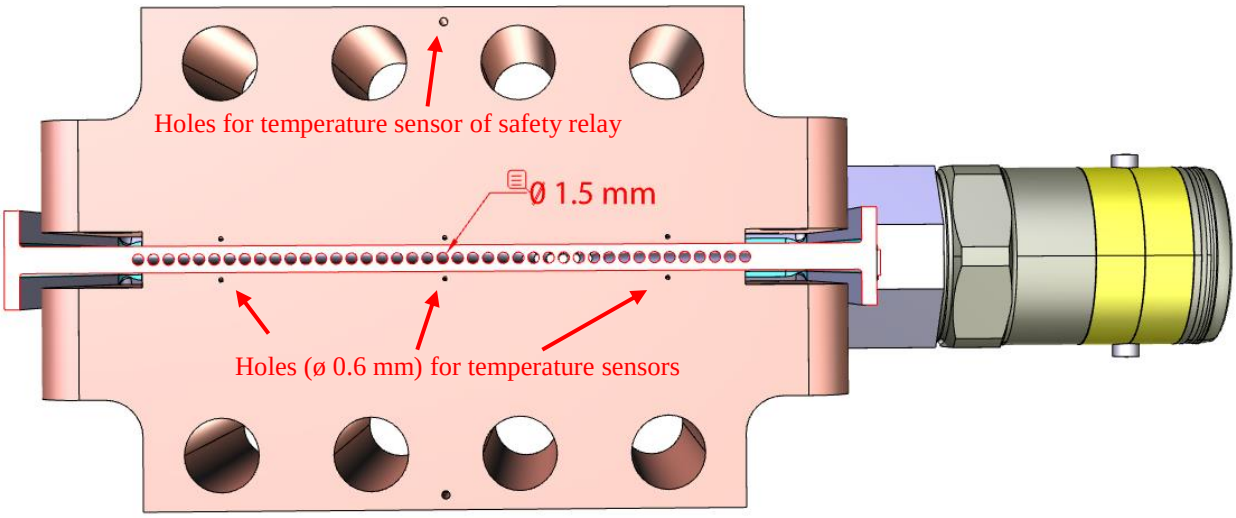

Figure 16: Cross-section of the evaporator plate with heater blocks mounted on both sides.

Figure 17: Photo of the coldplate.

DOI: 10.13009/EUCASS2023-539

4.2. Test setup

The NLR Two-Phase Test Facility (TPTF) is a two-phase Mechanically Pumped Fluid Loop that has been built by the NLR and is used for two-phase cooling component and concept testing. Figure 18 and Figure 19 are photos of the facility with and without thermal insulation. A further description of the TPTF is provided in [5]. A schematic drawing of the TPTF with the evaporator plate is shown in Figure 20. The TPTF has eight parallel branches to install evaporators, but in this test only one branch is used. The plate can be tested in two orientations; horizontal and with the manifolds in the vertical orientation. Figure 21 and Figure 22 show the evaporator plate in the test setup in horizontal position, while Figure 23 shows the evaporator plate in vertical position.
18 temperature sensors are inserted in the holes in the heater blocks (see Figure 13 and Figure 16 for the location of the holes for the temperature sensors) to measure the temperatures in the heater blocks. The locations of the temperature sensors are indicated in Figure 24.

Figure 18: Photo of the Test Facility without insulation.

Figure 19: Photo of the Test Facility with insulation.

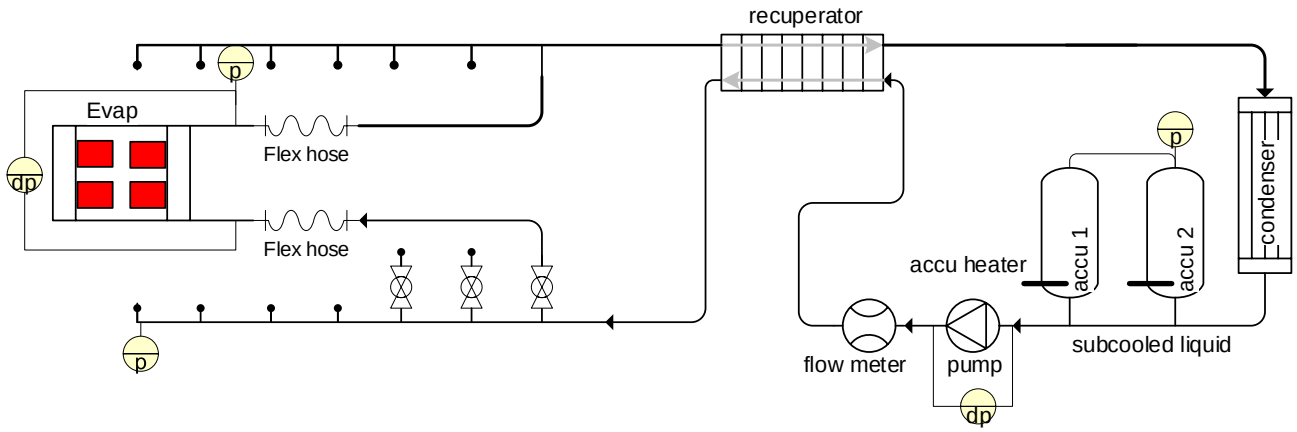

Figure 20: Schematic drawing of the test setup.

DOI: 10.13009/EUCASS2023-539

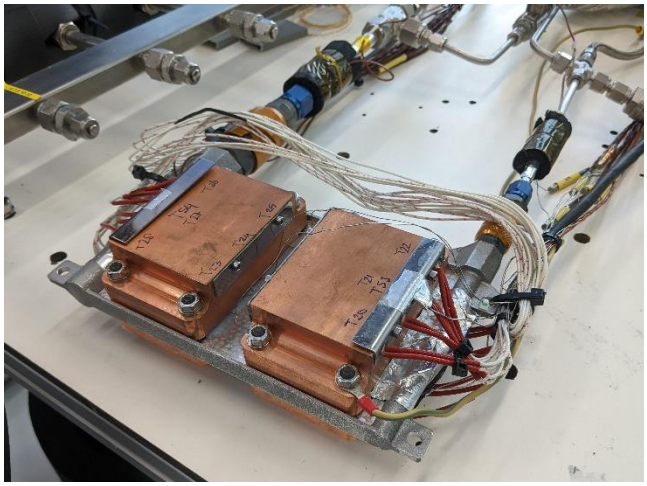

Figure 21: Photo of the evaporator plate in horizontal position without thermal insulation.

Figure 22: Photo of the evaporator plate in horizontal position with thermal insulation.

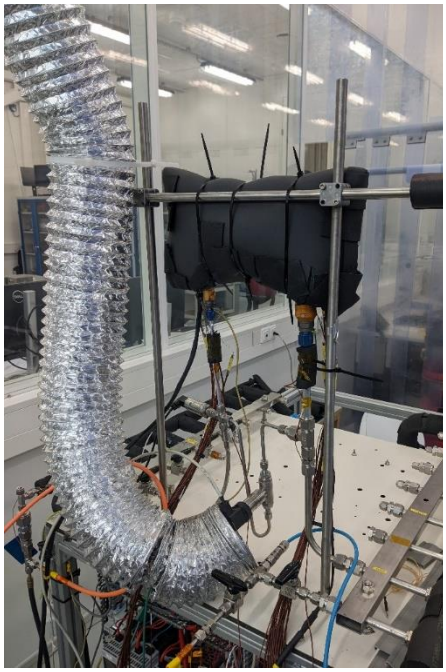

Figure 23: Photo of the evaporator plate in vertical position with thermal insulation.

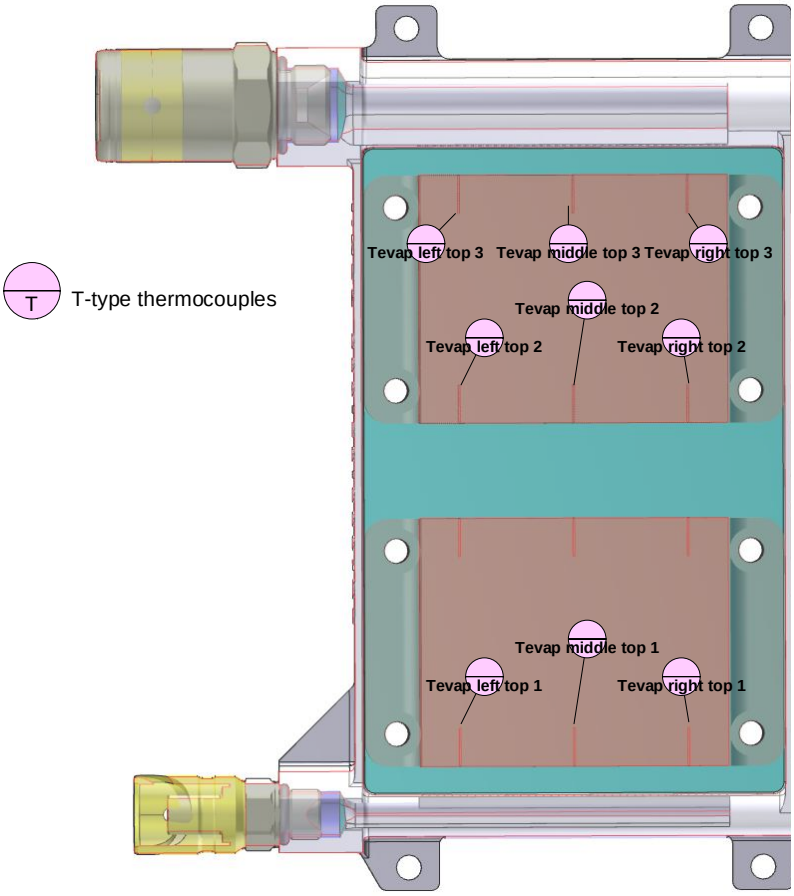

Figure 24: Cross-section with the location and name of the temperature sensors. There are 9 sensors on the top side of the coldplate (shown in figure) and 9 sensors on the corresponding location on the bottom side.

4.3. Test results

The system was first filled with R1233zd(E). The ordered R1233zd(E) was supposed to have a purity of >99.5%. However, after filling of the system it was noticed that an oily substance was mixed with the fluid. This was discussed with the supplier, and it was concluded that the R1233zd(E) vessel was indeed contaminated with an unknown substance. The R1233zdE container has been send back and will be replaced with high purity R1233zdE. However,

DOI: 10.13009/EUCASS2023-539

due to lead time and time constraints in the project, it was decided to perform the tests with R245fa instead, since R245fa has similar properties as R1233zd(E). In fact, R1233zd(E) has been developed as a drop-in replacement for R245fa, as an alternative with lower negative climate impact. After drainage of the R1233zd(E), and rinsing the system with IsoPropyl Alcohol (IPA) a few times for several hours to remove the oily substance, the system was filled with R245fa. The test results in horizontal and vertical orientation are described in the next sections.

Horizontal orientation

The coldplate performance test has been carried out in an automated test sequence with the following steps:

1. The saturation temperature in the system is increased to 75°C by using the accumulator heater. This takes approximately 30 minutes;
2. After one hour, the pump control is set to a mass flow of 36 g/s;
3. The heater blocks are set to 2000 W in total:
    a. 1000 W for bottom and 1000 W for top, for 1 hour;
    b. 0 W for bottom and 2000 W for top, for 0.5 hour;
    c. 2000 W for bottom and 0 W for top, for 0.5 hour;
    d. 1000 W for bottom and 1000 W for top, for 0.5 hour;
4. The heater blocks are set to 3000 W (1500 W for both top and bottom) for 0.5 hour;
5. The heater blocks are set to 4000 W (2000 W for both top and bottom) for 1.5 hour.

Figure 25 shows the measured massflow during the test. Figure 26 shows the measured heater powers. Figure 27 and Figure 28 show the absolute and differential pressures. Figure 29 shows the temperature at several locations, while Figure 30 shows the saturation temperature of the fluid (which is derived from the pressure at the evaporator outlet) and the temperatures of the 18 temperature sensors in the heater blocks on the evaporator plate. Figure 24 shows the location of these temperature sensors in the heater blocks. The sensor labels that end with index 1 are located near the inlet manifold of the evaporator and have a blue colour, while the sensor labels that end with index 3 are located near the outlet manifold and have a red colour. The measures temperatures by the sensors in between have a green colour. The measured temperatures from the sensors at the top side of the plate are indicated with solid lines while the dashed lines are used for the sensors at the bottom.

The saturation temperature in the system can be controlled by the heaters in the accumulator, which are regulated via a PID controller. When the temperature is lower than the setpoint, the accumulator heater power is increased, which increases the pressure and thereby the saturation temperate in the system. At the start of the measurement, the system saturation temperature is set to 75°C, of which the effects can be observed in Figure 26, Figure 27, and Figure 29. The accumulator heater is activated until a saturation temperature of 75°C is reached. The pump is then set to a flow of 36 g/s. 15 minutes after the pump is turned on, the evaporator heater blocks are set to a total heat input of 2000 W. The temperature of the heater blocks quickly rises until the saturation temperature is reached and the liquid starts to boil (see Figure 30). In steady-state with 2000 W (1000 W on both sides of the coldplate) all 18 sensors in the heater blocks have a temperature between 80 and 82°C. The fluid temperature is 75°C, so there is a temperature gradient ΔT of 5 to 7°C between the fluid and the heater blocks. Part of this ΔT is caused by the heat transfer between the fluid and the evaporator plate channel wall, and part of this ΔT is caused by the heat transfer between the evaporator plate and the copper block. In order to distinguish between these two effects, the 2000 W is only applied on only one side. The temperature sensors on the other side will then have approximately the same temperature as the evaporator plate. The temperature of the sensors in the heater block with no heat input is 78.2 to 79.0°C, which indicates a temperature difference between the fluid and the coldplate of 3.2 to 4.0°C. The temperature of the sensors in the heater block with 2000 W heat input is 82.2 to 83.6°C, which indicates a temperature difference between the coldplate and the heater blocks of 4.0 to 4.6°C. That means that more than half of the total temperature difference between the liquid and the heater blocks is caused by the temperature difference between the heater block and the coldplate.

When the heat input is increased to 4000 W and with a flow of 36 g/s, the vapour mass fraction is approximately 0.7. The measured heater block temperatures are between 83.4 and 86.2°C at this heat load, as shown in Figure 30.

When the evaporator heat input is initially set to 2000 W, the liquid temperature at the inlet of the evaporator rises to approximately 69°C, see ‘TevapIn’ in Figure 29. This is because the liquid that flows to the evaporator is warmed to a temperature close to the saturation temperature by the recuperator heat exchanger in the test setup, schematically shown in Figure 20.

DOI: 10.13009/EUCASS2023-539

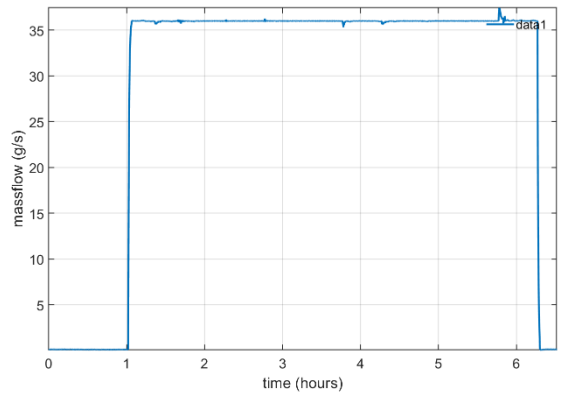

Figure 25: Measured massflow.

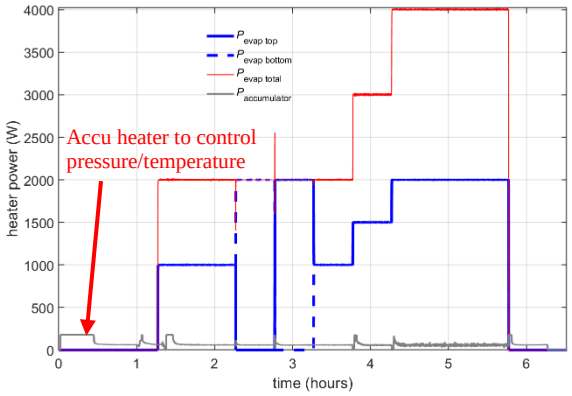

Figure 26: Measured heater power.

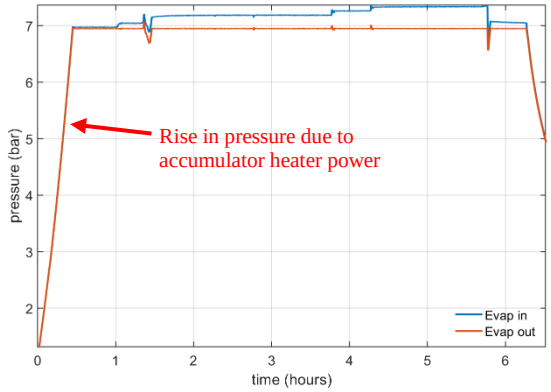

Figure 27: Measured absolute pressure.

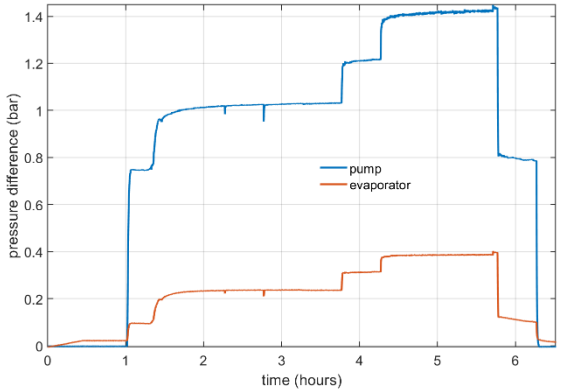

Figure 28: Measured pressure difference over the pump and evaporator.

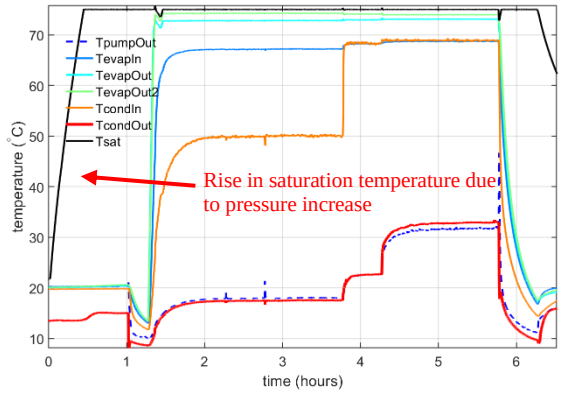

Figure 29: Measured temperatures at several locations.

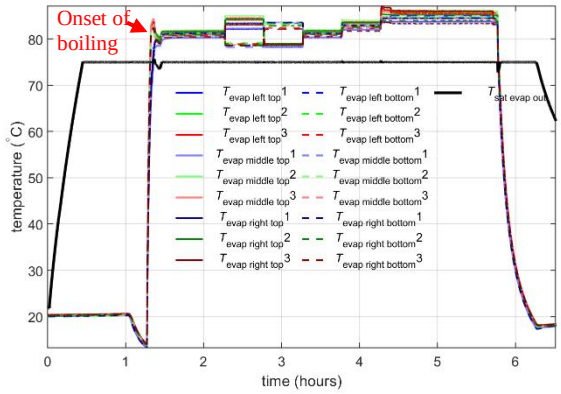

Figure 30: Measured temperatures on the evaporator plate.

Vertical orientation

Figure 31 shows the measured data for a test similar as the one described in the previous section, except that the plate is in the vertical orientation, see Figure 23 for a photo. The measured data is very similar to the data for the horizontal plate. From this it can be concluded that the change in orientation does not have an influence on the performance of the plate.

DOI: 10.13009/EUCASS2023-539

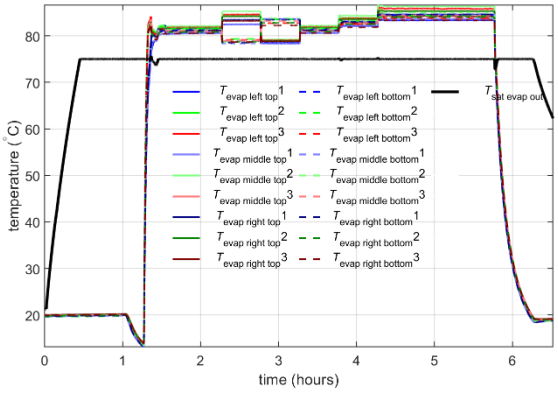

Figure 31: Measured temperatures on the evaporator plate in vertical orientation

5. Conclusion

In this study, we have successfully developed, manufactured and tested an additively manufactured AlSi10Mg coldplate for two-phase cooling of a DC/DC converter with 4 kW heat dissipation. R1233zd(E) was chosen as a working fluid for the cooling system. This coldplate with parallel channels successfully cooled a 4 kW heat load. With a saturation temperature of 75°C, the 18 temperature sensors on the power converter emulator all had a temperature between 83 and 86°C, indicating that the two-phase cooling results in a small temperature gradient and uniform temperature, despite the high heat flux. The coldplate was tested in different orientations, and no gravity effects were observed. Based on its shown performance in a lab environment, the technological maturity of the additively manufactured two-phase coldplate has been progressed to TRL4. With the advances made in this study, the coldplate enables significant performance and mass improvements compared to conventional liquid coldplates.

6. Acknowledgments

This project has received funding from the European Union's Horizon 2020 Research and Innovation programme under grant agreement No 875504. This publication reflects the authors' views. The European Union's Horizon 2020 Research and Innovation programme is not responsible for any use that may be made of the information.

7. References

[1] E. Lemmon, M. Huber and M. McLinden, "NIST Standard Reference Database 23: Reference Fluid Thermodynamic and Transport Properties-REFPROP", Version 9.1," *National Institute of Standards and Technology, Standard Reference Data Program, Gaithersburg.*

[2] F. P. Incropera, D. P. DeWitt, T. L. Bergman and A. S. Lavine, Fundamentals of heat and mass transfer, 6th edition, John Wiley & Sons, 2006.

[3] NFPA 704, "Standard System for the Identification of the Hazards of Materials for Emergency Response," [Online]. Available: https://www.nfpa.org/Codes-and-Standards/All-Codes-and-Standards/List-of-Codes-and-Standards. [Accessed 18 02 2021].

[4] H. J. Gerner and N. Braaksma, "Transient modelling of pumped two-phase cooling systems: Comparison between experiment and simulation, ICES-2016-004," in *46th International Conference on Environmental Systems*, 2016.

[5] H. J. van Gerner, R. Bolder and J. van Es, "Transient modelling of pumped two-phase cooling systems: Comparison between experiment and simulation with R134a, ICES-2017-037," in *47th International Conference on Environmental Systems*, 2017.

[6] L. Friedel, "Improved friction pressure drop correlation for horizontal and vertical two phase pipe flow," in *European Two Phase Flow Group Meeting*, Ispra, Italy, 1979.

[7] K. Gungor and R. Winterton, "Simplified general correlation for saturated flow boiling and comparisons of correlations with data," *The Canadian Journal of Chemical Engineering*, vol. 65, no. 148, 1987.

DOI: 10.13009/EUCASS2023-539

[8] M. Shah, “An Improved And Extended general Correlation for Heat Transfer During Condensation in Plain Tubes,” *HVAC&R Research,* vol. 15, pp. 889-913, 2009.

[9] “German agency seeks ban on R1233zd,” 15 8 2017. [Online]. Available: https://www.coolingpost.com/world-news/german-agency-seeks-ban-on-r1233zd/. [Accessed 11 12 2019].

[10] “PFAS ban affects most refrigerant blends,” 12 February 2023. [Online]. Available: https://www.coolingpost.com/world-news/pfas-ban-affects-most-refrigerant-blends/. [Accessed 20 April 2023].

[11] I. Moir and A. Seabridge, Aircraft Systems, Mechanical, Electrical, and Avionics Subsystems Integration, John Wiley & Sons Inc., 2008.

[12] IATC, “B737 NG Air Systems,” International Aviation Theory Centre, [Online]. Available: https://www.slideshare.net/theoryce/b737-ng-air-systems. [Accessed 1 February 2021].

[13] “Chemical Compatibility Database,” Cole-Parmer, [Online]. Available: https://www.coleparmer.com/chemical-resistance. [Accessed 11 12 2019].

[14] “Chemical Compatibility Guide,” Graco , [Online]. Available: https://www.graco.com/gb/en/products/ad/chemical-compatibility.html. [Accessed 11 12 2019].